

Odor Representations in Olfactory Cortex: “Sparse” Coding, Global Inhibition, and Oscillations

Cindy Poo¹ and Jeffry S. Isaacson^{1,*}

¹Department of Neuroscience, School of Medicine, University of California, San Diego, La Jolla, CA 92093, USA

*Correspondence: jisaacson@ucsd.edu

DOI 10.1016/j.neuron.2009.05.022

SUMMARY

The properties of cortical circuits underlying central representations of sensory stimuli are poorly understood. Here we use *in vivo* cell-attached and whole-cell voltage-clamp recordings to reveal how excitatory and inhibitory synaptic input govern odor representations in rat primary olfactory (piriform) cortex. We show that odors evoke spiking activity that is sparse across the cortical population. We find that unbalanced synaptic excitation and inhibition underlie sparse activity: inhibition is widespread and broadly tuned, while excitation is less common and odor-specific. “Global” inhibition can be explained by local interneurons that receive ubiquitous and nonselective odor-evoked excitation. In the temporal domain, while respiration imposes a slow rhythm to olfactory cortical responses, odors evoke fast (15–30 Hz) oscillations in synaptic activity. Oscillatory excitation precedes inhibition, generating brief time windows for precise and temporally sparse spike output. Together, our results reveal that global inhibition and oscillations are major synaptic mechanisms shaping odor representations in olfactory cortex.

INTRODUCTION

The functional properties of cortical circuits play a critical role in the central representations of sensory stimuli. However, the synaptic mechanisms governing stimulus-selective spike output in sensory cortices are still debated. Broadly tuned (lateral) inhibition is a fundamental physiological mechanism often proposed to sharpen responses to preferred stimuli, primarily by counteracting weak, nonpreferred excitatory input (Hartline et al., 1956; Priebe and Ferster, 2008). Surprisingly, intracellular studies in visual, auditory, and somatosensory cortex find that synaptic excitation and inhibition are cotuned to the same stimuli and inhibition elicited by nonpreferred stimuli is often weak (Anderson et al., 2000; Priebe and Ferster, 2008; Wehr and Zador, 2003; Wilentz and Contreras, 2005), suggesting that primary sensory cortical circuits lack properties supporting lateral inhibition.

Although the initial steps underlying the processing of olfactory information are beginning to be revealed, how olfactory

information is represented in the cortex is not well established. In rodents, olfactory information is initially processed in the olfactory bulb, where olfactory sensory neurons expressing one of ~1000 different types of odorant receptors map onto ~1800 glomeruli (Mombaerts et al., 1996). Within each glomerulus, 50–100 mitral and tufted (M/T) cells receive input from sensory neurons expressing a unique type of odorant receptor, and M/T cells are thought to represent particular odorant molecular features (Rubin and Katz, 1999; Uchida et al., 2000; Wachowiak and Cohen, 2001). Recent studies suggest that the spatial and temporal patterns of M/T cell activity encode the initial representations of olfactory information in the brain (Bathellier et al., 2008; Margrie and Schaefer, 2003; Rinberg et al., 2006; Soucy et al., 2009; Spors and Grinvald, 2002). However, odor perception ultimately requires the integration of M/T cell activity in higher cortical brain regions, and the synaptic mechanisms underlying cortical odor representations are unknown.

In this study, we explore the mechanisms governing odor representations in the anterior piriform cortex, a three-layered cortical region that plays a critical role in odor discrimination, recognition, and memory (Neville and Haberly, 2004; Wilson et al., 2006). Layer 2/3 (L2/3) pyramidal cells in anterior piriform cortex receive direct sensory input from M/T cell axons via the lateral olfactory tract (LOT), excitatory inputs from other cortical neurons, and inhibition via local GABAergic circuits (Figure 1A; Neville and Haberly, 2004). Individual L2/3 pyramidal cells likely receive converging input from M/T cells belonging to different glomeruli (Franks and Isaacson, 2006). Consistent with this idea, histochemical and extracellular studies suggest that individual odors can activate spatially distributed ensembles of neurons, and individual neurons may respond to multiple odors (Illig and Haberly, 2003; Litaudon et al., 2003; Rennaker et al., 2007; Wilson et al., 2006; Zou et al., 2005).

Here we use *in vivo* cell-attached and whole-cell recordings to reveal how excitatory and inhibitory synaptic input govern odor representations in L2/3 cells of rat primary olfactory cortex. We show that odor-evoked firing activity is sparse and distributed across the cortical neuron population. We find that unbalanced synaptic excitation and inhibition underlie sparse odor representations. Across the cortical population, odor-evoked inhibition is widespread while excitation is less common. In individual cells, excitation is odor-specific and inhibition is nonselective. We show that this “global” inhibition likely arises from local interneurons that receive broadly tuned excitation. We also find that odors evoke fast beta-frequency (15–30 Hz) oscillations in synaptic activity. Oscillating excitation precedes inhibition, generating

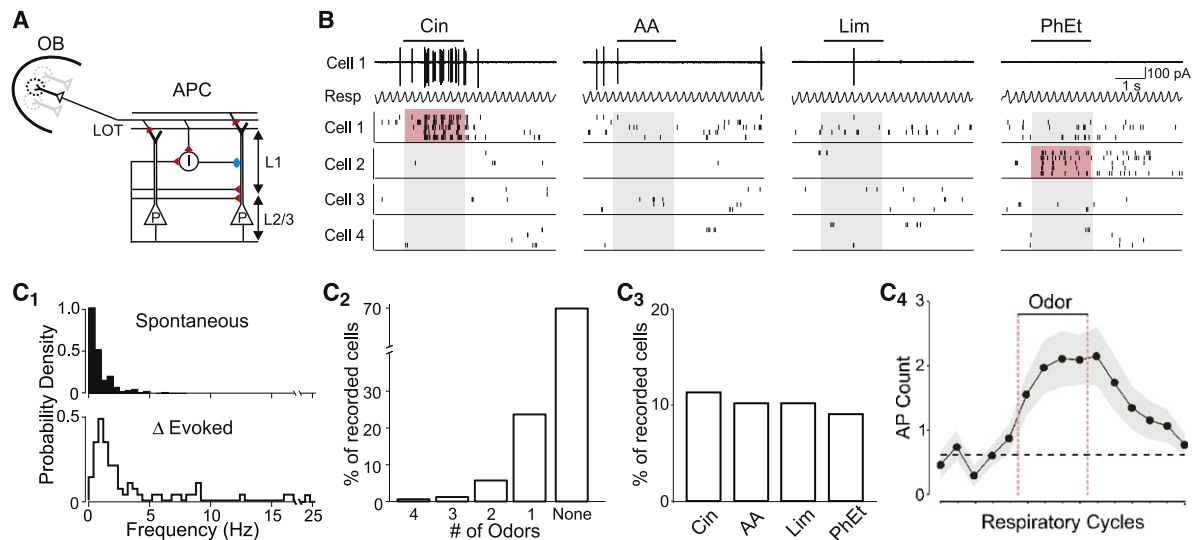


Figure 1. Odor-Evoked Action Potential Responses Are Sparse in Olfactory Cortex

(A) Schematic of anterior piriform cortex (APC). Olfactory bulb (OB) M/T cells project axons via the lateral olfactory tract (LOT) onto L2/3 pyramidal cells (P) and local interneurons (I). Red: excitatory synapses; blue: inhibitory synapses. (B) Raster plots of spikes from four representative cells. Top traces: cell-attached recording of spikes from Cell 1 and simultaneously monitored respiratory rhythm (Resp). Upward deflections in respiration trace correspond to inhalation. Bars indicate odor delivery (2 s) and pink shading indicates evoked responses. (C₁) Distributions of spontaneous AP frequency (top, $n = 177$ cells) and odor-evoked increases in firing rate (bottom, 72 responsive odor-cell pairs). (C₂) Distribution of odor selectivity. (C₃) Population response to individual odors. (C₄) Mean spike count for each respiratory cycle ($n = 72$ responsive odor-cell pairs). Dashed black line: mean spike count preceding odor delivery. Odors: cineole (Cin), amyl acetate (AA), R-limonene (Lim), phenylethyl alcohol (PhEt).

a brief (~ 10 ms) temporal window that restricts spike timing. Together, these results reveal that global inhibition and oscillatory synaptic inputs govern the tuning and timing of odor-evoked activity in olfactory cortex.

RESULTS

Odor-Evoked Spikes Are Sparse in Olfactory Cortex

We first investigated odor representations *in vivo* using cell-attached recordings of action potentials (APs) from anterior piriform cortex L2/3 neurons in urethane-anesthetized, freely breathing rats ($n = 59$). This recording method provides exceptional isolation of single units and is not biased toward the sampling of active or responsive cells (Hromadka et al., 2008; Margrie et al., 2002). Cell-attached recordings revealed low spontaneous firing rates of L2/3 cells (Figures 1B and 1C₁; median 0.28 Hz, mean 0.73 ± 0.08 Hz, $n = 177$ cells) and APs were frequently time-locked to the ~ 2 Hz respiratory rhythm (Buonviso et al., 2006; Litaudon et al., 2003; Rennaker et al., 2007) (Figures 1B and S1, available online).

Results from a large set of individually sampled neurons ($n = 177$) were used to infer the distribution of odor-evoked firing activity across the cortical population. In order to determine how individual stimuli are represented by the cortical population, we sampled responses to a small, fixed odor set rather than searching for the optimal stimulus for a particular neuron. We tested four monomolecular odors (5% saturated vapor [SV]) with unique and distinct structures and perceptual qualities: cineole (ether, eucalyptus), amyl acetate (ester, banana), R-limonene (terpene, citrus), and phenylethyl alcohol (alcohol, floral).

For each odor tested in every cell (odor-cell pair), we used both changes in mean firing rate and the reliability of firing across trials to categorize activity as odor-evoked or nonresponsive (see Experimental Procedures). Although we observed clear odor-evoked suppression of APs in some cells ($n = 9$ cells, data not shown), the low spontaneous firing rate precluded accurate classification of inhibitory responses.

We first determined the odor selectivity of individual cells, as well as the population response to each individual odor. In other words, we tested the number of odors each cell responded to, and the number of cells each odor can activate. For cells with odor-evoked responses (55/177), most (42/55) fired selectively to only one of the four odors (Figure 1C₂). In terms of the population response, each odor evoked activity in $\sim 10\%$ of tested cells (Figure 1C₃), indicating that the different odors elicited spikes in relatively small fractions of the cortical population. Interestingly, despite their structural diversity, each unique odor activated very similar fractions (range 9%–11%) of the cortical population.

To better understand the distribution of odor-evoked activity in olfactory cortex, we explored the intensity of stimulus-evoked responses. For responsive odor-cell pairs, the average increase in firing rate during the odor stimulus (2 s) was 2.01 ± 0.04 Hz (Figure 1C₁; range 0.05–24.5 Hz; median: 0.83 Hz, $n = 72$ odor-cell pairs). Strong responses were rarely observed: only 19% of responses exceeded 5 Hz and very few (6%) exceeded 10 Hz (Figure 1C₁). Evoked APs were coupled strongly to the respiratory rhythm (Figures 1B and S1), and on average odors evoked only an additional 1.6 ± 0.04 spikes (median: 0.6 AP) above baseline during each respiratory cycle throughout the odor stimulus (Figure 1C₄). Thus, odor responses consisted of weak increases

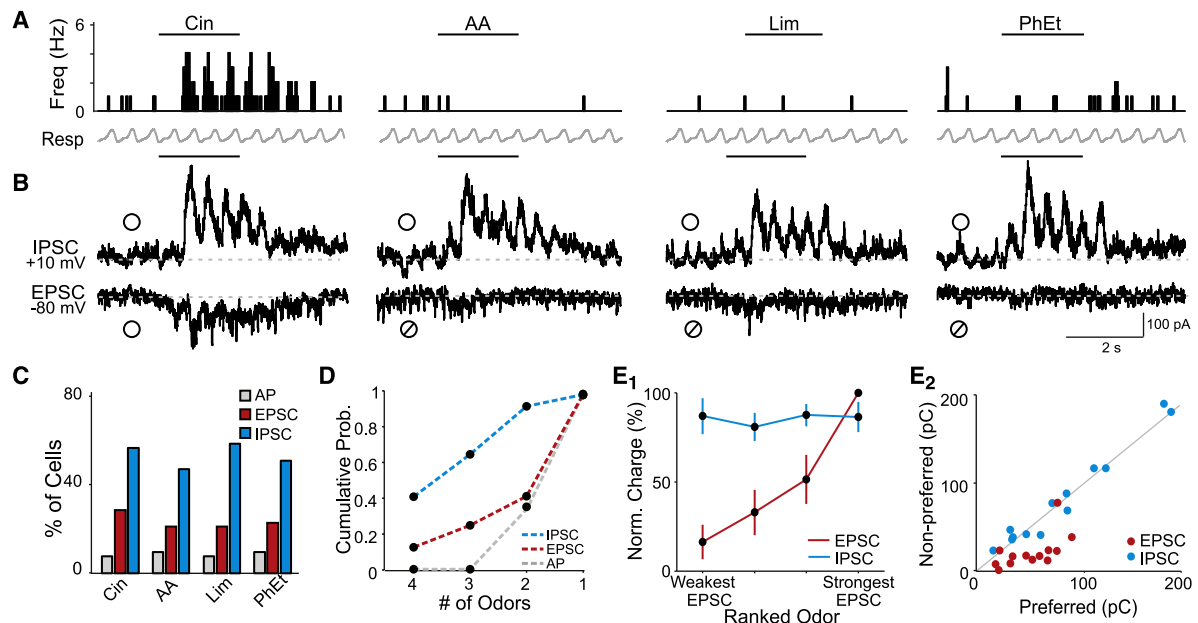


Figure 2. Odors Evoke Widespread and Nonselective Inhibition

(A) Peristimulus time histogram of APs recorded in cell-attached mode from a single cell. Bars indicate odor delivery. (B) Subsequent voltage-clamp recording of excitation (EPSC) and inhibition (IPSC) from the same cell in (A). O, odor response; Ø, lack of response. Traces are averages of five trials. (C) Population responses to four odors ($n = 52$ cells). (D) Cumulative probability distribution of odor selectivity for each cell. (E₁) Normalized and ranked odor-evoked EPSC charge for cells with odor-evoked APs. IPSC charge (normalized to the strongest inhibitory response in each cell) is plotted for each of the corresponding odors ranked by EPSC strength ($n = 13$ cells). (E₂) EPSC and IPSC charge for odors that evoked spikes (Preferred) versus odors that did not generate spikes (Non-preferred) in the same cells ($n = 13$ cells). Odors: cineole (Cin), amyl acetate (AA), R-limonene (Lim), phenylethyl alcohol (PhEt).

in firing rate in the majority of responsive cells, while a small fraction of neurons fired more strongly.

In addition to quantifying odor selectivity and the population response in terms of odor-cell pairs that were categorized as odor-evoked or nonresponsive, we also used statistical measures calculated from raw firing rate distributions (Rolls and Tovee, 1995; Willmore and Tolhurst, 2001). This provides a description of odor-evoked activity without relying on binary categorization of responses. Lifetime sparseness (S_L , range 0 to 1 = highly selective), a measure of how an individual cell responds to multiple stimuli (see Experimental Procedures), indicated that cells responded selectively (S_L mean = 0.88 ± 0.002 , median = 1, $n = 177$ cells). Population sparseness (S_p , range 0 to 1 = most sparse), a measure of how an individual stimulus is represented across a population, was also high (mean $S_p = 0.93$, range 0.90–0.96). Taken together, our results indicate that odor representations are sparse in olfactory cortex.

Global Inhibition and Selective Excitation Underlie Sparse Odor Representations

What governs the sparse population response of L2/3 cells? To address this question, we used *in vivo* whole-cell recording (Marrig et al., 2002) to examine the synaptic input underlying spike output in an additional set of L2/3 cells ($n = 52$). Following cell-attached recording of APs (Figure 2A), excitatory and inhibitory postsynaptic currents (EPSCs and IPSCs, respectively) were recorded in voltage-clamp mode in each cell (Figure 2B). EPSCs were recorded at -80 mV, the reversal potential for inhibition

set by our internal solution (chloride reversal potential $[E_{Cl}] = -80$ mV). Similarly, IPSCs were recorded at the reversal potential for excitation ($\sim +10$ mV). In the absence of applied odors, cells received barrages of spontaneous EPSCs (77 ± 12 Hz) and IPSCs (57 ± 10 Hz, $n = 12$ representative cells, data not shown), and odors evoked synaptic currents that were coupled to the respiration cycle (Figures 2B and S1). We first examined synaptic responses categorically and determined responsiveness (the presence or absence of odor-evoked activity) for each odor-cell pair from the increase in charge transfer during odor presentation (see Experimental Procedures).

We first compared the fractions of cells in this population that responded to the different odors with APs, EPSCs, and IPSCs. Each of the different odors elicited responses in similar fractions of cells (Figure 2C). We estimated population sparseness from the fraction of cells responsive to each odor averaged over all odors. While cells with odor-evoked APs were rarely observed ($8.3\% \pm 0.5\%$ of the population), odor-evoked excitation was more common ($22.7\% \pm 1.5\%$) and inhibition was remarkably widespread ($51.8\% \pm 2.2\%$, Figure 2C). Furthermore, S_p calculated from unthresholded synaptic charge measurements during odor presentation indicated that excitatory synaptic responses ($S_p = 0.72 \pm 0.03$) were significantly sparser than inhibition ($S_p = 0.56 \pm 0.02$, $p = 0.006$). These results suggest that across the cortical population, ubiquitous odor-evoked inhibition contributes to firing activity that is more sparsely distributed than synaptic excitation.

We further explored whether inhibition contributes to sparse odor-evoked firing activity by blocking fast synaptic inhibition

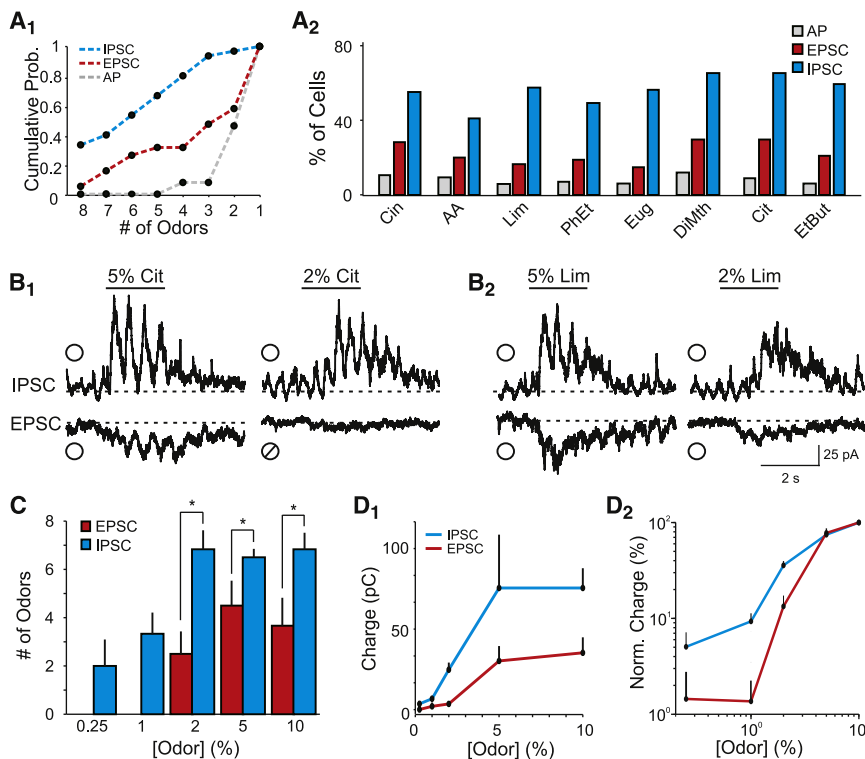


Figure 3. Global Inhibition Is Not Dependent on Odor Identity and Persists over a Range of Concentrations

(A₁) Cumulative probability distribution of odor selectivity for cells tested with eight odors ($n = 34$ cells). (A₂) Population response of APs, EPSCs, and IPSCs for all cells ($n = 86$ cells). (B) Representative average EPSCs and IPSCs from an L2/3 cell in response to two odors (B₁ and B₂) at 5% and 2% saturated vapor (SV). O indicates a positive odor response; Ø indicates a negative odor response. (C) Number of odors that evoked excitation and inhibition in cells tested with eight odors over a range of concentrations. Cells with excitatory responses to multiple odors at 5% SV were selected for these experiments. Each cell was tested with all odors at five concentrations ($n = 9$ cells, $*p < 0.05$). (D₁) Odor-evoked increases in EPSC and IPSC charge across odor concentrations. (D₂) Normalized odor-evoked charge for EPSCs (red) and IPSCs (blue) plotted on a log-log scale. Odors: cineole (Cin), amyl acetate (AA), R-limonene (Lim), phenylethyl alcohol (PhEt), eugenol (Eug), dimethyl pyrazidine (DiMth), citral (Cit), and ethyl butyrate (EtBut).

with the GABA_A receptor antagonist gabazine (SR-95531). However, local cortical superfusion of gabazine (20–100 μ M) led to epileptic activity evident as ictal bursts (~ 1 Hz) of spikes in cell-attached recordings ($n = 10$). Once epileptic events began, odor-evoked activity was lost and spikes became decoupled from respiration. Nonetheless, in two experiments we observed a broadening in the odor tuning of firing activity in the presence of gabazine before the cortex became epileptic (under control conditions the two cells fired in response to only one of four odors versus two and three odors in the presence of drug; data not shown).

We next considered the odor selectivity of synaptic excitation and inhibition in individual cells. Although cells with odor-evoked EPSCs were more common than APs (Figure 2C), EPSCs were selectively evoked by only one out of four odors in the majority of cells (60%, Figure 2D). Strikingly, inhibition was recruited non-selectively; in 66% of cells that received inhibition, it was evoked by three or all four odors (Figure 2D). Together, these findings suggest that inhibition is global in olfactory cortex, i.e., odors evoke widespread inhibition across the population, and inhibition within an individual cell is broadly tuned to odors.

If inhibition were truly global in olfactory cortex, we would predict that the relative strength of inhibition evoked by different odors would be more uniform than excitation in individual cells. To address this, we examined the relative strength of excitation and inhibition in all cells that fired APs in response to odors ($n = 13$). Excitation (EPSC charge) elicited by each odor was normalized to the largest odor-evoked excitatory response in each cell. Inhibition (IPSC charge) was normalized similarly. Responses in each cell were then ranked from the odor that produced the weakest excitation to the odor that produced the strongest

and averaged across cells (Figure 2E₁). As we hypothesized for global inhibition, the strength of excitatory responses was graded, while the strength of inhibition was uniform across odors (Figure 2E₁).

Differing amounts of excitation and uniform inhibition imply that odors trigger APs based on the strength of excitation rather than odor-specific inhibition. Indeed, odors that elicited APs (preferred odors) also evoked greater excitation (average EPSC charge: 46.5 ± 1.5 pC) than those that failed to produce spikes (nonpreferred odors, 16.9 ± 0.7 pC, $p = 0.002$) in the same cells (Figure 2E₂). In contrast, preferred and nonpreferred odors evoked identical amounts of inhibition (Figure 2E₂; average IPSC charge: 78.6 ± 3.7 pC and 77.3 ± 1.7 pC, respectively, $p = 0.81$). Together, these results suggest that odor-evoked excitation must be strong enough to overcome global inhibition to generate APs in olfactory cortex.

To verify that our observations were not specific to our panel of test odors, we studied an additional set of cells ($n = 34$ cells) using double the number of odors. We observed the same relative relationships in the selectivity (Figure 3A₁) and population responses (Figure 3A₂) of odor-evoked activity, i.e., APs were evoked sparsely and selectively, synaptic excitation was more common but specific, and inhibition was widespread and most broadly tuned. In a subset of these cells, we also examined the relationship between synaptic excitation and inhibition across a range of odor intensities. We varied odor concentration for cells that responded with excitation to multiple odors at our standard concentration of 5% SV. We found that odors were much more likely to evoke inhibition compared to excitation across a range of concentrations (0.25%–10% SV). Reducing odor concentration from 5% to 2% SV led to a loss of excitatory responses to

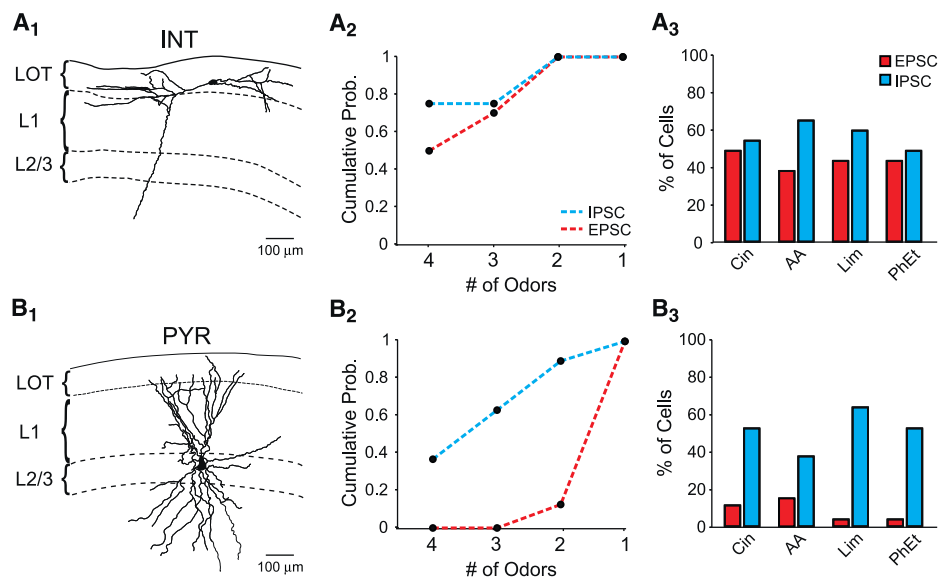


Figure 4. Interneurons Receive Widespread and Broadly Tuned Odor-Evoked Excitation

(A₁) Morphologically identified interneuron following *in vivo* recording. Only the soma and dendritic arbor are shown in reconstruction. (A₂) Selectivity of odor-evoked EPSCs and IPSCs in interneurons. (A₃) Interneuron population responses. (B₁) Morphologically identified pyramidal cell. Only the soma and dendritic arbor are shown in reconstruction. (B₂ and B₃) Pyramidal cell selectivity and population responses. Odors: cineole (Cin), amyl acetate (AA), R-limonene (Lim), phenylethyl alcohol (PhEt).

some odors while inhibitory responses to the same odors remained (Figures 3B and 3C; $n = 9$ cells). Indeed, as odor intensity was reduced further, odor-evoked inhibition could be observed in the absence of excitation (Figure 3C). Furthermore, when normalized to the maximal synaptic responses we recorded at 10% SV, the relative amplitudes (charge) of inhibition at low odor concentrations were greater than those of excitation (Figure 3D). Thus, inhibition is preferentially recruited across a wide range of odor intensities. Together, these results provide strong evidence that global inhibition is a fundamental property of olfactory cortical circuits.

Excitation onto Local Interneurons Is Broadly Tuned

What accounts for global inhibition in olfactory cortex? One possibility is that, unlike principal cells, the local interneurons underlying inhibition receive widespread and broadly tuned excitation. To address this question, we filled cells with biocytin during whole-cell recording for post hoc classification. Interneurons were targeted by recording from cells in layer 1 (Neville and Haberly, 2004). Indeed, synaptic excitation was largely nonselective in morphologically identified interneurons (Figures 4A₁ and 4A₂; $n = 18$ cells), while identified pyramidal cells received selective excitation (Figures 4B₁ and 4B₂; $n = 27$ cells) similar to results from our larger L2/3 population. On average, individual odors evoked excitation in a greater fraction of interneurons compared to pyramidal cells (Figures 4A₃ and 4B₃; interneurons: $50\% \pm 3.9\%$; pyramidal cells: $11\% \pm 2.3\%$, $p = 0.003$) and inhibition was recruited similarly in both cell types ($p = 0.2$). These findings suggest that nonselective odor-evoked excitation of local interneurons could underlie global inhibition.

One mechanism that could lead to broadly tuned excitation onto interneurons is the receipt of a higher convergence of olfac-

tory bulb M/T cell inputs than pyramidal cells. We examined this possibility *in vivo* by placing a stimulating electrode in the LOT to directly activate M/T cell axons and recording LOT-evoked responses in L2/3 cells (Figure 5A). At high stimulus intensities, LOT stimulation evoked monosynaptic EPSCs (Figure 5B₁) at a holding potential of -80 mV. We then lowered stimulus strength to reduce the number of recruited axons such that stimulation failed to evoke EPSCs (Figure 5B₂). Changing the membrane potential to $+10$ mV revealed LOT-evoked IPSCs at the same stimulus intensity that failed to evoke EPSCs (Figure 5B₃). Subsequent application of the glutamate receptor antagonist NBQX ($500 \mu\text{M}$) to the cortical surface abolished the IPSCs, indicating that they were evoked disynaptically (Figure 5B₃). The onset times of IPSCs evoked with this “minimal” stimulation lagged behind monosynaptic EPSCs in the same cells (Figure 5C), further confirming their disynaptic nature (Pouille and Scanziani, 2001). Disynaptic IPSCs could routinely be recruited in the absence of LOT-evoked EPSCs (Figure 5D, $n = 5$). These experiments suggest that interneurons governing inhibition in olfactory cortex receive a higher convergence of M/T cell input than pyramidal cells.

Oscillatory Synaptic Inputs Govern Spike Timing

In sensory cortices receiving balanced excitation and inhibition, excitation precedes inhibition in response to brief impulse-like stimuli. This difference in the relative timing of excitation and inhibition is proposed to shape stimulus selectivity and precisely timed spike output (Priebe and Ferster, 2008; Wehr and Zador, 2003; Wilent and Contreras, 2005). In the mammalian olfactory system, respiratory modulation is a prominent feature governing the time course of odor-evoked activity (Cang and Isaacson, 2003; Litaudon et al., 2003; Margrie and Schaefer, 2003; Rennaker

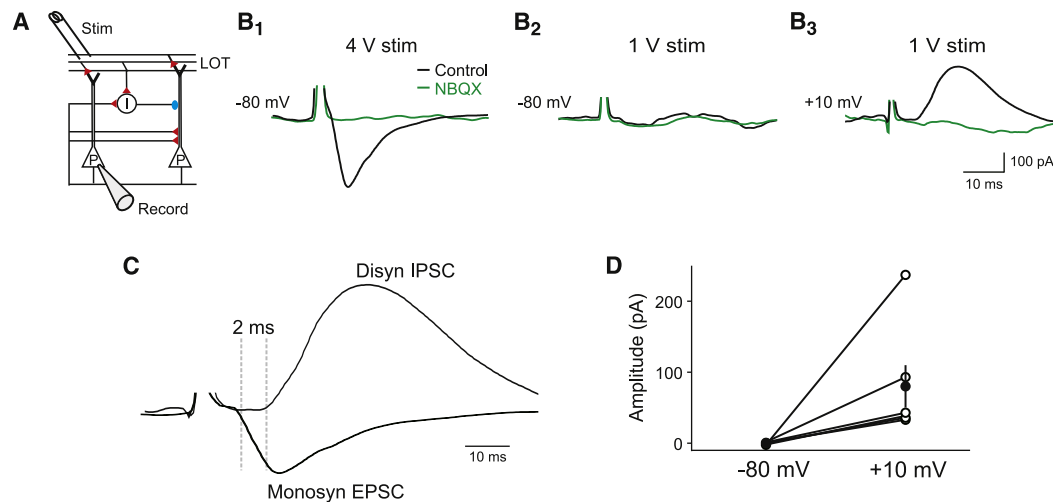


Figure 5. Minimal Stimulation of the LOT In Vivo Preferentially Recruits Disynaptic Inhibition

(A) Schematic of recording setup. (B₁) Under control conditions, direct LOT stimulation evokes a monosynaptic EPSC ($V_m = -80$ mV) at high stimulation intensity (4 V) in an L2/3 cell. (B₂) Lowering stimulation intensity (1 V) fails to evoke an EPSC, while depolarization to +10 mV reveals an IPSC (B₃). Subsequent application of NBQX (500 μ M) to the cortical surface abolishes the monosynaptic EPSC and disynaptic IPSC (B₁–B₃, green traces). (C) Overlay of monosynaptic EPSC and disynaptic IPSC. (D) Summary data of recruitment of disynaptic IPSCs (+10 mV) at stimulus intensities that failed to evoke EPSCs (–80 mV, $n = 5$ cells).

et al., 2007). We wondered whether the temporal relationship between odor-evoked excitation and inhibition could account for the timing of respiratory-coupled APs (Figure 6A₁). However, aligning odor-evoked synaptic currents to the respiratory rhythm revealed that inhibition and excitation were temporally overlapping (Figures 6A and 6B; $n = 12$ cells), and we could not resolve an obvious relationship between synaptic inputs and spikes times.

What then determines spike timing during slow, respiratory-coupled barrages of synaptic activity? Synchronized activity of ensembles of neurons is known to generate odor-evoked oscillations in local field potentials (LFPs) and phase-locked APs in higher olfactory centers of vertebrates and invertebrates (Adrian, 1942; Eeckman and Freeman, 1990; Freeman, 1978; Litaudon et al., 2008; Perez-Orive et al., 2002). To explore a temporal relationship between APs and synaptic input of L2/3 cells that may exist on a finer timescale than respiration, we recorded odor-evoked LFPs in layer 1 of anterior piriform cortex.

We found prominent, odor-evoked beta-frequency oscillations (mean = 18.0 ± 1.7 Hz, $n = 10$ rats) in the LFP (Figure 7A), consistent with previous studies of behaving and anesthetized rats (Chapman et al., 1998; Lowry and Kay, 2007; Neville and Haberly, 2003). Beta oscillations were qualitatively similar for different odors and coupled to respiration (Figure 7B₁). Simultaneous cell-attached recording of L2/3 cells and the LFP revealed that APs were phase locked to LFP beta oscillations (Figure 7B). In all cells, odor-evoked APs were coherent with the LFP at beta frequencies (Figure 7C, $n = 9$ cells). Intriguingly, the peaks of perioscillation triggered spike histograms (POTHs) (Figure 7D₁) indicated that APs were not coupled to the same phases of the beta oscillation across different cells. Rather, APs in each individual cell were preferentially coupled to specific phases of the LFP oscillation (Figure 7D₂, $n = 7/9$ cells, Rayleigh test, $p < 0.05$). LFP oscillations simultaneously recorded at the most rostral and caudal edges of anterior piriform cortex (~ 2.5 mm

apart) were virtually coincident (lag: 1.2 ms, 0.11 radians), ruling out the possibility that cell-specific AP-LFP phase relationships reflected varying distances between the site of LFP and AP recording. Furthermore, in cells that responded with APs to multiple odors ($n = 3$ cells), the AP-LFP phase relationship appeared identical for each odor (data not shown). These results showing precise phase relationships between APs in individual neurons and synchronized network oscillations point to a temporally sparse code for odor representations in olfactory cortex (Laurent, 2002).

Given the tight temporal association between APs and beta oscillations, we examined the relationship between odor-evoked intracellular synaptic responses and the LFP (Figures 8A₁ and 8A₂). We found that respiration-coupled barrages of EPSCs and IPSCs were coherent to the LFP at beta frequencies in all cells (Figure 8A₃; $n = 9$, $p < 0.05$, coherence confidence limit). LFP-triggered averages of synaptic currents revealed that EPSCs always preceded IPSCs on a brief, millisecond timescale (Figure 8B; average lag = 9 ± 0.3 ms). Strikingly, odor-evoked APs were largely confined to the narrow time windows when EPSCs led IPSCs in the same cells (Figures 8C and 8D; $n = 3$ cells). On average, $67\% \pm 11\%$ of APs during odor presentation occurred during the LFP period ($\sim 0.7 \pi$, 20 ms) corresponding to the time window between the onset of the EPSC and the 50% rise time of the IPSC. In contrast, only $32\% \pm 12\%$ of APs occurred during the same length of LFP period ($\sim 0.7 \pi$) when measured from the onset of the IPSC. In addition, only $8\% \pm 2\%$ of APs occurred during the LFP period ($\sim 0.4 \pi$, 13 ms) corresponding to the interval from the 50% rise time of the IPSC to the time of its peak. We also found that synaptic excitation and inhibition were always coupled to distinct phases of the LFP beta oscillation in each cell (Figure 8D, $n = 9$ cells), consistent with the cell-specific distribution of AP-LFP phases. Thus, while respiration imposes slow epochs of overlapping excitation and

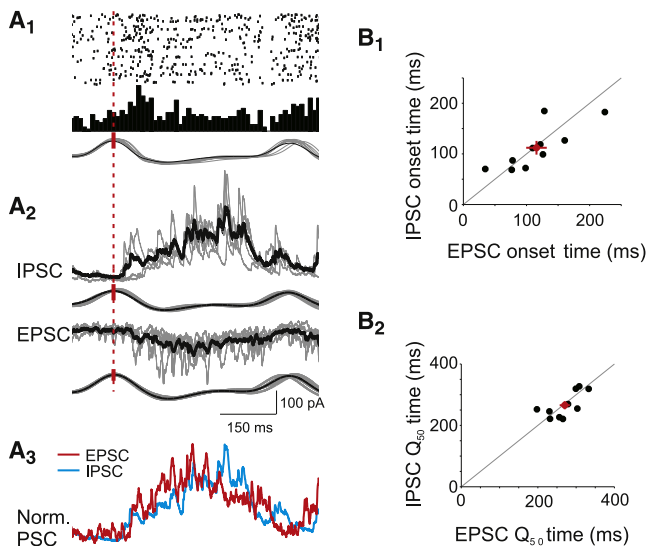


Figure 6. Respiration-Coupled Synaptic Excitation and Inhibition Temporally Overlap

(A₁) Raster plot (top) and peristimulus time histogram (middle) of odor-evoked APs aligned to respiration (bottom) from one cell. (A₂) Respiration-triggered average EPSC and IPSC for the cell in (A₁). Black trace, average current. Gray traces, single trials. Red dashed line notes the peak of inhalation to which responses were aligned. (A₃) Normalized respiration-triggered EPSC (red, inverted) and IPSC (blue) have overlapping time courses. (B) Respiration-triggered EPSCs and IPSCs have similar onset times (B₁) and time to 50% of charge transfer (B₂) in individual cells ($n = 12$ cells).

inhibition, odors evoke rapidly oscillating synaptic currents. Phase differences in oscillating EPSCs and IPSCs enforce precise spike timing in olfactory cortex.

DISCUSSION

In this study, we show that odor representations are sparse in olfactory cortex. We find that sparse population activity is governed by selective excitation and global inhibition. Interneurons receiving widespread and broadly tuned excitation are poised to mediate global inhibition. We also explore the timing of odor-evoked spikes. We find that, in addition to slow respiratory patterning, spikes in principal cells are coupled to fast, beta-frequency oscillations in the LFP. These precise and temporally sparse spikes are generated by oscillatory synaptic excitation that leads inhibition.

“Sparse” Cortical Odor Representations

We wished to understand how neuronal populations in olfactory cortex represent individual odors. In other words, what is the typical response of the cortical population to a particular odor? Our approach differs from those that study representations of sensory stimuli by searching for the optimal stimulus for each cell, i.e., to define the “receptive field” of particular neurons. Measuring receptive fields is problematic in olfactory cortex since the number of odors that can potentially be encoded is vast and the topographical mapping of odor space within the

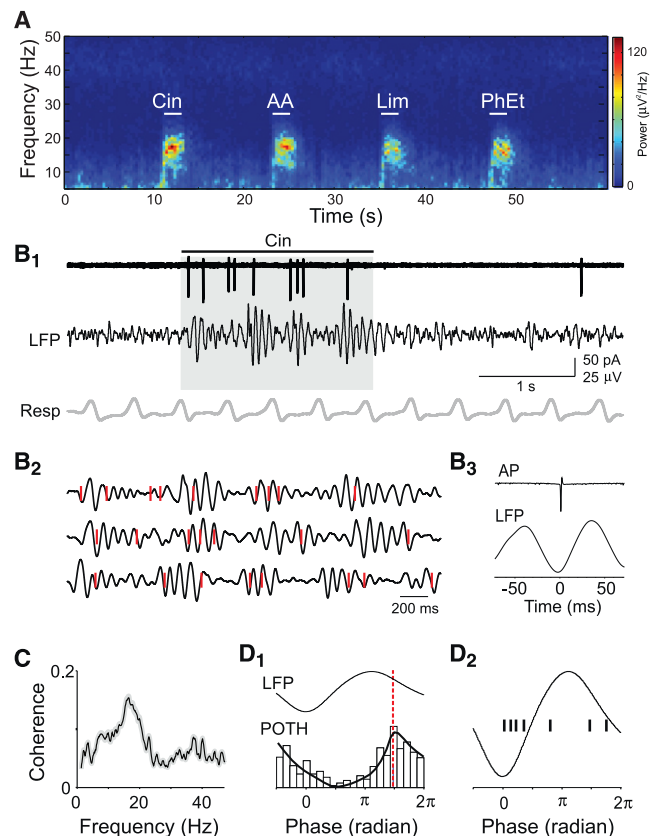


Figure 7. Odor-Evoked Spikes Are Phase Locked to Beta-Frequency LFP Oscillations

(A) Spectrogram of an LFP recording showing beta oscillations evoked by four odors. (B₁) Simultaneously recorded odor-evoked APs (top), LFP (filtered at 5–30 Hz), and respiration. (B₂) Expansion of gray-shaded period in (B₁) (top trace) and two other trials. Red ticks indicate APs. (B₃) Spike-triggered average LFP from the same cell. (C) Average coherence between odor-evoked APs and LFPs ($n = 9$ cells). (D₁) POTH of odor-evoked spikes from cell shown in (B) superimposed with a local linear fit. Red dashed line indicates peak of POTH used to determine AP-LFP phase. (D₂) AP-LFP phase relationships (black ticks) for seven cells.

cortex is unknown. Here, we used a small, fixed set of odors and data from individually recorded cells to reconstruct the overall population response. This approach allowed us to infer how individual stimuli (odors) are represented across the cortical population. A similar strategy has been used to explore the nature of stimulus representations in the insect olfactory system (Perez-Orive et al., 2002; Szyszka et al., 2005; Turner et al., 2008) and mammalian auditory cortex (Hromadka et al., 2008).

In contrast to extracellular unit recording, cell-attached recordings are not biased toward the detection of neurons with high firing rates. We used this method to sample the distribution of firing rates in olfactory cortex. We find that L2/3 cells in vivo have very low spontaneous activity (<1 Hz) and individual odors caused an increase in firing in ~10% of the cortical population. This is consistent with the idea that unique odors are represented by ensembles of active cells and that these cells are distributed similarly across the cortical population.

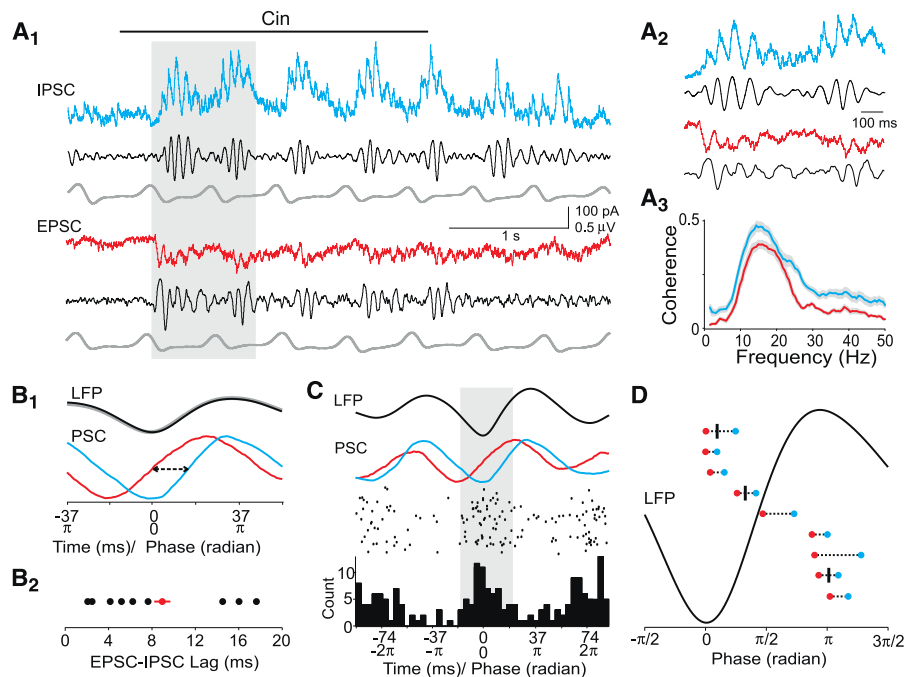


Figure 8. Oscillating Excitatory and Inhibitory Synaptic Currents Govern Spike Timing

(A₁) Simultaneous recording of synaptic currents and LFP. Gray-shaded period is expanded in (A₂). (A₃) Average coherence between odor-evoked synaptic currents and LFPs ($n = 9$ cells). (B₁) LFP oscillation-triggered average EPSC (red) and IPSC (blue) from cell in (A). EPSC is shown inverted. Arrows: lag time measured as interval between EPSC and IPSC 50% rise times (T_{50}). (B₂) Summary of EPSC-IPSC lag time for nine cells. (C) Top traces: LFP and oscillation-triggered EPSC and IPSC. Bottom panels: perioscillation triggered raster and spike histogram for the same cell. (D) Summary of EPSC-IPSC timing relative to LFP phase for nine cells. Red: EPSC T_{50} ; blue: IPSC T_{50} . AP-LFP phase relationships (black ticks) are shown superimposed for the three cells that fired APs in response to odors.

Given that individual odors can activate 10% of the cortical population, is it valid to describe odor representations as “sparse” in piriform cortex? It is important to bear in mind that the odor responses of “active” cells were extremely weak. For responsive cells, odor-evoked increases in firing rate averaged only 2 Hz and only 6% of these cells had “well-driven” responses (>10 Hz). While we tested odors at a moderate concentration of 5% SV, it is likely that at lower concentrations even fewer cells within the cortical population would be active. Low spontaneous and evoked firing rates have also been reported in other cortical regions from anesthetized and awake animals when activity is measured using patch-clamp recording techniques (Brecht and Sakmann, 2002; DeWeese et al., 2003; Hromadka et al., 2008; Margrie et al., 2002). Together, the low firing rates, the small fraction of the population activated by individual odors, and the rarity of well-driven responses indicate that odor representations are sparse in olfactory cortex (Laurent, 2002; Olshausen and Field, 2004; Rolls and Tovee, 1995; Willmore and Tolhurst, 2001).

It has been reported that responses of olfactory bulb mitral cells to odorants are weaker and less frequently observed in awake, behaving animals compared to ketamine/xylazine-anesthetized animals (Rinberg et al., 2006). Thus, odor representations in the olfactory bulb can be sparser in awake animals versus those in the anesthetized state. While our experiments were performed under urethane anesthesia, a lower level of

odor-evoked mitral cell activity may lead to sparser cortical odor representations in the awake, behaving state.

Global Inhibition

Extracellular and immunohistological studies suggest that odors can activate ensembles of cells that are spatially dispersed (Illig and Haberly, 2003; Rennaker et al., 2007). The distribution of odor-evoked activity in olfactory cortex is fundamentally determined by the convergence (Franks and Isaacson, 2006) and divergence of M/T cell axon collaterals (Ojima et al., 1984). Anatomical studies suggest that single M/T cell axons terminate in broad, overlapping patches of olfactory cortex (Buonviso et al., 1991; Ojima et al., 1984). In addition, associative connections between pyramidal cells can amplify and further distribute excitation across the cortical population (Neville and Haberly, 2004; Rennaker et al., 2007). How does the olfactory cortical network counterbalance broadly distributed afferent excitatory input and highly associative connections to accomplish sparse odor-evoked spiking activity?

We propose that global inhibition is a major feature governing sparse odor representations in olfactory cortex. In contrast to the balanced excitation and inhibition elicited by stimuli in other primary sensory cortices (Anderson et al., 2000; Priebe and Ferster, 2008; Tan et al., 2004; Wehr and Zador, 2003; Wilent and Contreras, 2005), odor-evoked inhibition is widespread and nonselective in olfactory cortex. Global inhibition is poised to

dampen odor-evoked excitatory responses across olfactory cortex such that only cells receiving strong and preferred excitation are driven to spike. In addition to promoting sparseness, global inhibition can contribute to cortical odor coding by providing gain control, noise suppression, and state-dependent modulation of cortical activity (Hensch and Fagiolini, 2004; Murakami et al., 2005).

We show that global inhibition is likely to reflect the fact that local interneurons receive ubiquitous odor-evoked excitation that is broadly tuned. We suggest that broadly tuned excitation of olfactory cortex interneurons is due to a higher convergence of M/T cell inputs to interneurons than principal cells. In support of this idea, we found that low-intensity LOT stimulation consistently evoked disinaptic inhibition in the absence of excitation in pyramidal cells. While feedforward interneurons in olfactory cortex are likely to play an important role (Luna and Schoppa, 2008), local feedback circuits may also contribute to global inhibition.

Oscillating Synaptic Inputs Govern Spike Timing

Neuronal oscillations are thought to be an important feature that contributes to the processing of information in cortical networks (Buzsaki and Draguhn, 2004; Salinas and Sejnowski, 2001). Fast rhythmic activity in the LFP is well documented in the olfactory systems of both vertebrates and invertebrates (Adrian, 1942; Chapman et al., 1998; Eeckman and Freeman, 1990; Freeman, 1978; Friedrich et al., 2004; Lowry and Kay, 2007; Neville and Haberly, 2003; Perez-Orive et al., 2002; Wehr and Laurent, 1996) and synchronous activity of neural ensembles is proposed to be important for odor coding, discrimination, and learning (Laurent, 2002).

We found that odors evoked respiration-coupled, beta-frequency oscillations in the olfactory cortex LFP. Although the precise mechanisms underlying beta-frequency oscillations are unclear, they are thought to involve bidirectional connectivity between olfactory bulb and cortex (Neville and Haberly, 2003) and have been implicated during olfactory behavior (Kay and Stopfer, 2006). We show that while firing activity of individual L2/3 cells is slowly modulated by respiration, spike timing is precisely phase locked to beta-frequency oscillations in the LFP. Furthermore, individual cells prefer to spike at different phases of the LFP beta oscillation. Thus, across the cell population and within each breath, odors evoke spikes that are temporally sparse (Laurent, 2002).

What determines the LFP phase at which individual cells spike? Using whole-cell voltage-clamp recordings, we show that cells receive excitatory and inhibitory currents coupled to discrete phases of the beta oscillation cycle. Inhibition always lagged excitation on a millisecond timescale and this temporal offset between oscillating EPSCs and IPSCs generated brief time windows governing spike timing. Thus, despite relatively slow respiratory patterning, rapidly oscillating synaptic activity enforces precise spike timing in olfactory cortex. Our results suggest that spike timing is important for odor representations in olfactory cortex and raises the intriguing possibility that cell-specific spike timing within active ensembles of L2/3 cells contributes to odor coding in brain regions receiving L2/3 projections.

Intriguingly, many of our findings parallel those obtained in the locust mushroom body (Laurent, 2002), a structure positioned at

an equivalent stage of the insect olfactory system, but which shares no obvious homology or evolutionary relationship with the mammalian piriform cortex. The pyramidal cell equivalent in the mushroom body is the Kenyon cell and the similarities include: lifetime and population sparseness of principal cell responses, very low response firing rate deviation from baseline, direct and specific excitatory drive, broadly tuned inhibition, stimulus-triggered bursts of beta-range oscillations, and a phase delay of inhibition relative to excitation. Indeed, there are relatively few functional differences across these diverse phyla. In locusts, broadly tuned inhibition of mushroom body Kenyon cells is mediated by feedforward interneurons located in another region, the lateral horn (Perez-Orive et al., 2002). In the piriform cortex, broadly tuned inhibition is generated locally by feedforward and perhaps feedback interneurons. While Kenyon cells fire spikes with a similar mean phase relationship to odor-evoked LFPs (Perez-Orive et al., 2002) recorded in the antenna lobe (the equivalent of the mammalian olfactory bulb), we find that the firing phase of individual pyramidal cells relative to the LFP varies across all cells. Overall, the remarkable similarities between the two different systems may reflect fundamental principles governing the processing of olfactory information in higher brain regions.

Sparse representations of stimuli have been found across a variety of sensory systems (Brecht and Sakmann, 2002; Davison and Katz, 2007; Hahnloser et al., 2002; Hromadka et al., 2008; Margrie et al., 2002; Perez-Orive et al., 2002; Rinberg et al., 2006; Vinje and Gallant, 2000). Sparseness is proposed to promote the efficient coding of sensory information in the brain by having a relatively small fraction of neurons within a large population active at any given time (Hromadka et al., 2008; Laurent, 2002; Olshausen and Field, 2004; Rolls and Tovee, 1995; Willmore and Tolhurst, 2001). Global inhibition and synchronized oscillatory synaptic currents are well suited to generate odor representations in olfactory cortex that are both spatially and temporally sparse.

Sparse coding is suggested to be an efficient means for representing sensory stimuli and is advantageous for associative learning (Laurent, 2002; Olshausen and Field, 2004). Thus, this coding scheme is ideal for the olfactory cortex given the immensity of potential odors and its importance for odor learning, recognition, and classification (Wilson et al., 2006). Indeed, in the insect olfactory system as well as the mammalian olfactory bulb, sparse activity is thought to be critical in the coding of odors (Davison and Katz, 2007; Fantana et al., 2008; Laurent, 2002; Perez-Orive et al., 2002; Rinberg et al., 2006). Our results suggest that sparse coding may be a fundamental strategy of olfactory systems that is highly conserved across diverse species.

EXPERIMENTAL PROCEDURES

Surgical Procedure

All animal experiments were performed in strict accordance with the guidelines of the National Institutes of Health and the University of California Institutional Animal Care and Use Committee. Sprague Dawley rats (p16–21) were anesthetized with urethane (1.8 g/kg) supplemented with atropine (0.2 mg/kg). Skin incisions were infused with lidocaine. Similar results were found in animals anesthetized with ketamine ($n = 3$ cells, data not shown). Body

temperature was maintained at 35°C–37°C and animals were head-fixed on a custom stereotaxic fixture. After removing a section of temporomandibular muscle, the LOT was visualized through the ventral surface of the skull. A small (~1 mm²) craniotomy was made lateral to the rhinal sulcus, ~1 mm caudal to the middle cerebral artery, and dorsal to the top edge of the LOT to expose the anterior piriform cortical surface. A larger craniotomy (~5 mm²) was made when LFPs were simultaneously recorded. For LOT stimulation experiments, an additional craniotomy was made ~1.5 mm anterior to the recording site. Respiration was monitored with a chest-mounted piezoelectric strap.

Odor Stimuli

Odors were delivered via a computer-controlled olfactometer with a 1 l/min constant flow. Odors were diluted 1:10 in mineral oil, and further diluted with charcoal-filtered air to achieve a 5% SV in most experiments unless otherwise noted. Odors were presented ~1 cm from the snout in pseudorandomized order. Odors were presented for 2 s with 60 s between presentations of individual odors. Odors were: cineole, amyl acetate, R-limonene, phenylethyl alcohol, eugenol, dimethyl pyrazidine, citral, and ethyl butyrate.

Electrophysiology

Cell-attached and whole-cell recordings were made with patch pipettes (5–7 MΩ) filled with (in mM) 130 cesium gluconate, 5 NaCl, 10 HEPES, 0.2 EGTA, 12 phosphocreatine, 3 Mg-ATP, and 0.2 Na-GTP (7.25 pH; 290–300 mOsm). For data collected using only cell-attached recordings (*n* = 177 cells), neurons were distinguished from glia or other nonneuronal structures by only considering cases in which at least one AP was detected over several minutes of recording. EPSCs were recorded at –80 mV, the reversal potential for inhibition set by our internal solution (*E*_{Cl} = –80 mV). Similarly, IPSCs were recorded at the reversal potential for excitation (~+10 mV). Series resistance for whole-cell recording was ≤30 MΩ and continuously monitored. Cells in which series resistance changed by >10% were excluded. L2/3 or layer 1 cells were targeted based on the *z* axis readout of an MP-285 micromanipulator (Sutter). A stimulating electrode (FHC) placed within the LOT was used for LOT-evoked synaptic responses. LFPs were recorded using a tungsten electrode (FHC) in layer 1a ~0.5 mm anterior to the patch electrode recording site.

Histology

Biocytin (0.2%) was added to the internal solution for experiments with post hoc histological reconstruction. Briefly, after electrophysiology recordings, an overdose of urethane was given to the animal, after which the animal was decapitated and the whole brain extracted and fixed in 4% paraformaldehyde in 0.1 M phosphate-buffered saline. The recorded hemisphere was then sectioned into 200 μm parasagittal slices. To recover biocytin-filled cells in whole-mount, cells were revealed by a DAB reaction with nickel intensification. Slices were dehydrated in alcohols and xylenes and mounted in damar resin. These cells were then manually reconstructed using NeuroLucida. Cells were identified as interneurons or pyramidal cells based on the following criteria: all layer 1 cells and L2/3 cells with a bipolar or multipolar dendritic tree were categorized as interneurons (Neville and Haberly, 2004). Pyramidal cells were identified as L2/3 cells possessing a clear apical dendrite and dendritic tree branching toward the LOT; in addition, cells must have had basal dendrites that were confined within L2/3 (Neville and Haberly, 2004).

Data Acquisition and Analysis

Recordings were made with a MultiClamp 700A (Molecular Devices), digitized at 5 kHz (Instrutech), and acquired using AxographX (Axograph). Data were analyzed using custom routines in Matlab (Mathworks). Power and coherence spectra with confidence limits were calculated using multitapered methods (Jarvis and Mitra, 2001) and the Chronux package (NIMH). Cells were included in analysis only if >3 odor presentation trials for APs, EPSCs, and IPSCs were obtained. To determine AP responses to odors, we measured APs during a baseline period (2 s) prior to the odor application and during the 2 s odor presentation. Spikes were counted in 200 ms bins. Given the low firing rates of L2/3 cells, we used a combination of two criteria to determine evoked spike activity: (1) average firing rate threshold and (2) spike reliability. Cell-odor pairs needed to satisfy both criteria in order to be categorized as “responsive.” For cells that had spontaneous APs, (1) average firing rate threshold: the average

firing rate during the 2 s odor presentation needed to exceed the mean baseline rate +2.5 standard deviations (SD) for ≥3 bins. (2) The firing rate in >50% of trials during odor presentation needed to exceed mean baseline firing rate +2.5 SD in ≥1 bin. We chose a threshold of 2.5 SD based on a simple receiver-operating characteristic (ROC) analysis (Fantana et al., 2008). Varying the threshold (in terms of mean firing rate + *X* SD) demonstrated that a threshold of 2.5 SD produces a true positive to false positive ratio of 93% (*n* = 177 cells). Thus, we were confident that our method was appropriate for sensitively detecting odor-evoked responses.

For cells with no spontaneous APs, (1) average firing rate threshold: the average firing rate during the 2 s odor presentation needed to exceed 0.5 Hz. (2) The firing rate in >50% of trials during odor presentations needed to exceed 0.5 Hz. The median spontaneous rate was 0.28 Hz, thus, 0.5 Hz was a conservative threshold. We find that varying this threshold from 0.25 to 1 Hz did not alter the number of responsive cell-odor pairs.

Average odor-evoked spiking activity and synaptic currents were aligned to the first inhalation cycle in the presence of odor. Odor-evoked synaptic activity was measured by calculating the charge transfer (*Q*_{odor}) during the 2 s odor presentation. Baseline response (*Q*_{baseline}) was calculated from a 2 s period preceding odor onset. The criteria for a “positive” odor-evoked synaptic response was defined as Response Index (RI) = (*Q*_{odor}/*Q*_{baseline}) ≥ 1.6. This threshold value was also derived from ROC analysis of varying RI thresholds to obtain the optimal threshold producing a true positive to false positive ratio of >90% (Figure S2).

To eliminate ambiguity inherent to binary classification of odor-cell pairs as responsive or nonresponsive, we used an additional selectivity measurement: *S*_L (Rolls and Tovee, 1995; Willmore and Tolhurst, 2001), which is independent of detection threshold. In brief, *S*_L was calculated as $(1 - \{[S^N_j r_j / N] / [S^N_j r_j^2 / N]\}) / (1 - 1/N)$, where *r_j* was the response of the neuron to odorant *j* (mean firing rate or charge transfer during odor presentation), and *N* was the total number of odors. This provides a measure of how much the response of a neuron was attributable entirely to one odor (highly selective, *S*_L = 1) versus equally distributed across all odors (*S*_L = 0). *S*_p was calculated with the same method; however, *r_j* was the response of cell *j* to a single odor, and *N* was the total number of cells tested with this odor. In this case, *S*_p provides a measure of how much of the total population response was attributed entirely to one cell (highly sparse, *S*_p = 1) versus equally distributed across all cells (*S*_p = 0).

Beta oscillations were detected by digitally filtering the LFP between 8–30 Hz, which did not result in any phase shift, as confirmed by comparing beta troughs in filtered and raw traces. The oscillation cycle amplitude was defined as the peak-to-trough amplitude, i.e., the difference between the peaks of a given cycle to the subsequent trough of the same cycle. Events with amplitudes ≥4 SD from the mean were detected. The POTHs for spikes and oscillation-triggered average for synaptic currents were determined using a method similar to spike-triggered averaging. In this case, however, the average was triggered by the trough of an oscillation cycle recorded in the LFP. Rayleigh test of no-uniformity was used for the POTH in each cell to evaluate significance of AP-LFP phase coupling. The POTH was fitted with a local linear regression (Chronux) in order to extract the peak firing time during an LFP oscillation cycle.

The phase lag between EPSC and IPSC for each cell was accessed in two ways: time lag between the oscillation-triggered EPSC and IPSC transformed into phase as well as the phase lag between LFP-EPSC and LFP-IPSC at peak coherence. Both methods yielded identical results. Summary data and error bars are presented as mean ± SEM and statistical analysis was performed with paired *t* tests unless otherwise noted.

SUPPLEMENTAL DATA

Supplemental data for this article include two Supplemental Figures and can be found at [http://www.cell.com/neuron/supplemental/S0896-6273\(09\)00397-3](http://www.cell.com/neuron/supplemental/S0896-6273(09)00397-3).

ACKNOWLEDGMENTS

We are grateful to B. Atallah, R. Malinow, M. Scanziani, and C. Zuker for advice and encouragement. This work was supported by NIDCD (R01DC04682, J.S.I.) and NRSA (5F31DC009366, C.P.).

Accepted: May 13, 2009

Published: June 24, 2009

REFERENCES

- Adrian, E.D. (1942). Olfactory reactions in the brain of the hedgehog. *J. Physiol.* 100, 459–473.
- Anderson, J.S., Carandini, M., and Ferster, D. (2000). Orientation tuning of input conductance, excitation, and inhibition in cat primary visual cortex. *J. Neurophysiol.* 84, 909–926.
- Bathellier, B., Buhl, D.L., Accolla, R., and Carleton, A. (2008). Dynamic ensemble odor coding in the mammalian olfactory bulb: sensory information at different timescales. *Neuron* 57, 586–598.
- Brecht, M., and Sakmann, B. (2002). Dynamic representation of whisker deflection by synaptic potentials in spiny stellate and pyramidal cells in the barrels and septa of layer 4 rat somatosensory cortex. *J. Physiol.* 543, 49–70.
- Buonviso, N., Revial, M.F., and Jourdan, F. (1991). The Projections of Mitral Cells from Small Local Regions of the Olfactory Bulb: An Anterograde Tracing Study Using PHA-L (Phaseolus vulgaris Leucoagglutinin). *Eur. J. Neurosci.* 3, 493–500.
- Buonviso, N., Amat, C., and Litaudon, P. (2006). Respiratory modulation of olfactory neurons in the rodent brain. *Chem. Senses* 31, 145–154.
- Buzsaki, G., and Draguhn, A. (2004). Neuronal oscillations in cortical networks. *Science* 304, 1926–1929.
- Cang, J., and Isaacson, J.S. (2003). In vivo whole-cell recording of odor-evoked synaptic transmission in the rat olfactory bulb. *J. Neurosci.* 23, 4108–4116.
- Chapman, C.A., Xu, Y., Haykin, S., and Racine, R.J. (1998). Beta-frequency (15–35 Hz) electroencephalogram activities elicited by toluene and electrical stimulation in the behaving rat. *Neuroscience* 86, 1307–1319.
- Davison, I.G., and Katz, L.C. (2007). Sparse and selective odor coding by mitral/tufted neurons in the main olfactory bulb. *J. Neurosci.* 27, 2091–2101.
- DeWeese, M.R., Wehr, M., and Zador, A.M. (2003). Binary spiking in auditory cortex. *J. Neurosci.* 23, 7940–7949.
- Eeckman, F.H., and Freeman, W.J. (1990). Correlations between unit firing and EEG in the rat olfactory system. *Brain Res.* 528, 238–244.
- Fantana, A.L., Soucy, E.R., and Meister, M. (2008). Rat olfactory bulb mitral cells receive sparse glomerular inputs. *Neuron* 59, 802–814.
- Franks, K.M., and Isaacson, J.S. (2006). Strong single-fiber sensory inputs to olfactory cortex: implications for olfactory coding. *Neuron* 49, 357–363.
- Freeman, W.J. (1978). Spatial properties of an EEG event in the olfactory bulb and cortex. *Electroencephalogr. Clin. Neurophysiol.* 44, 586–605.
- Friedrich, R.W., Habermann, C.J., and Laurent, G. (2004). Multiplexing using synchrony in the zebrafish olfactory bulb. *Nat. Neurosci.* 7, 862–871.
- Hahnloser, R.H., Kozhevnikov, A.A., and Fee, M.S. (2002). An ultra-sparse code underlies the generation of neural sequences in a songbird. *Nature* 419, 65–70.
- Hartline, H.K., Wagner, H.G., and Ratliff, F. (1956). Inhibition in the eye of *Limulus*. *J. Gen. Physiol.* 39, 651–673.
- Hensch, T.K., and Fagioli, M. (2004). Excitatory-Inhibitory Balance: Synapses, Circuits, Systems (New York: Kluwer Academic/Plenum).
- Hromádka, T., Deweese, M.R., and Zador, A.M. (2008). Sparse representation of sounds in the unanesthetized auditory cortex. *PLoS Biol.* 6, e16.
- Illig, K.R., and Haberly, L.B. (2003). Odor-evoked activity is spatially distributed in piriform cortex. *J. Comp. Neurol.* 457, 361–373.
- Jarvis, M.R., and Mitra, P.P. (2001). Sampling properties of the spectrum and coherency of sequences of action potentials. *Neural Comput.* 13, 717–749.
- Kay, L.M., and Stopfer, M. (2006). Information processing in the olfactory systems of insects and vertebrates. *Semin. Cell Dev. Biol.* 17, 433–442.
- Laurent, G. (2002). Olfactory network dynamics and the coding of multidimensional signals. *Nat. Rev. Neurosci.* 3, 884–895.
- Litaudon, P., Amat, C., Bertrand, B., Vigouroux, M., and Buonviso, N. (2003). Piriform cortex functional heterogeneity revealed by cellular responses to odours. *Eur. J. Neurosci.* 17, 2457–2461.
- Litaudon, P., Garcia, S., and Buonviso, N. (2008). Strong coupling between pyramidal cell activity and network oscillations in the olfactory cortex. *Neuroscience* 156, 781–787.
- Lowry, C.A., and Kay, L.M. (2007). Chemical factors determine olfactory system beta oscillations in waking rats. *J. Neurophysiol.* 98, 394–404.
- Luna, V.M., and Schoppa, N.E. (2008). GABAergic circuits control input-spike coupling in the piriform cortex. *J. Neurosci.* 28, 8851–8859.
- Margrie, T.W., and Schaefer, A.T. (2003). Theta oscillation coupled spike latencies yield computational vigour in a mammalian sensory system. *J. Physiol.* 546, 363–374.
- Margrie, T.W., Brecht, M., and Sakmann, B. (2002). In vivo, low-resistance, whole-cell recordings from neurons in the anaesthetized and awake mammalian brain. *Pflügers Arch.* 444, 491–498.
- Mombaerts, P., Wang, F., Dulac, C., Chao, S.K., Nemes, A., Mendelsohn, M., Edmondson, J., and Axel, R. (1996). Visualizing an olfactory sensory map. *Cell* 87, 675–686.
- Murakami, M., Kashiwadani, H., Kirino, Y., and Mori, K. (2005). State-dependent sensory gating in olfactory cortex. *Neuron* 46, 285–296.
- Neville, K.R., and Haberly, L.B. (2003). Beta and gamma oscillations in the olfactory system of the urethane-anesthetized rat. *J. Neurophysiol.* 90, 3921–3930.
- Neville, K.R., and Haberly, L.B. (2004). *Olfactory Cortex*, Fifth Edition (New York: Oxford University Press).
- Ojima, H., Mori, K., and Kishi, K. (1984). The trajectory of mitral cell axons in the rabbit olfactory cortex revealed by intracellular HRP injection. *J. Comp. Neurol.* 230, 77–87.
- Olshausen, B.A., and Field, D.J. (2004). Sparse coding of sensory inputs. *Curr. Opin. Neurobiol.* 14, 481–487.
- Perez-Orive, J., Mazor, O., Turner, G.C., Cassenaer, S., Wilson, R.I., and Laurent, G. (2002). Oscillations and sparsening of odor representations in the mushroom body. *Science* 297, 359–365.
- Pouille, F., and Scanziani, M. (2001). Enforcement of temporal fidelity in pyramidal cells by somatic feed-forward inhibition. *Science* 293, 1159–1163.
- Priebe, N.J., and Ferster, D. (2008). Inhibition, spike threshold, and stimulus selectivity in primary visual cortex. *Neuron* 57, 482–497.
- Rennaker, R.L., Chen, C.F., Ruyle, A.M., Sloan, A.M., and Wilson, D.A. (2007). Spatial and temporal distribution of odorant-evoked activity in the piriform cortex. *J. Neurosci.* 27, 1534–1542.
- Rinberg, D., Koulakov, A., and Gelperin, A. (2006). Sparse odor coding in awake behaving mice. *J. Neurosci.* 26, 8857–8865.
- Rolls, E.T., and Tovee, M.J. (1995). Sparseness of the neuronal representation of stimuli in the primate temporal visual cortex. *J. Neurophysiol.* 73, 713–726.
- Rubin, B.D., and Katz, L.C. (1999). Optical imaging of odorant representations in the mammalian olfactory bulb. *Neuron* 23, 499–511.
- Salinas, E., and Sejnowski, T.J. (2001). Correlated neuronal activity and the flow of neural information. *Nat. Rev. Neurosci.* 2, 539–550.
- Soucy, E.R., Albeanu, D.F., Fantana, A.L., Murthy, V.N., and Meister, M. (2009). Precision and diversity in an odor map on the olfactory bulb. *Nat. Neurosci.* 12, 210–220.
- Spors, H., and Grinvald, A. (2002). Spatio-temporal dynamics of odor representations in the mammalian olfactory bulb. *Neuron* 34, 301–315.
- Szyska, P., Ditzgen, M., Galkin, A., Galizia, C.G., and Menzel, R. (2005). Sparsening and temporal sharpening of olfactory representations in the honeybee mushroom bodies. *J. Neurophysiol.* 94, 3303–3313.
- Tan, A.Y., Zhang, L.I., Merzenich, M.M., and Schreiner, C.E. (2004). Tone-evoked excitatory and inhibitory synaptic conductances of primary auditory cortex neurons. *J. Neurophysiol.* 92, 630–643.
- Turner, G.C., Bazhenov, M., and Laurent, G. (2008). Olfactory representations by *Drosophila* mushroom body neurons. *J. Neurophysiol.* 99, 734–746.
- Uchida, N., Takahashi, Y.K., Tanifuji, M., and Mori, K. (2000). Odor maps in the mammalian olfactory bulb: domain organization and odorant structural features. *Nat. Neurosci.* 3, 1035–1043.

- Vinje, W.E., and Gallant, J.L. (2000). Sparse coding and decorrelation in primary visual cortex during natural vision. *Science* 287, 1273–1276.
- Wachowiak, M., and Cohen, L.B. (2001). Representation of odorants by receptor neuron input to the mouse olfactory bulb. *Neuron* 32, 723–735.
- Wehr, M., and Laurent, G. (1996). Odour encoding by temporal sequences of firing in oscillating neural assemblies. *Nature* 384, 162–166.
- Wehr, M., and Zador, A.M. (2003). Balanced inhibition underlies tuning and sharpens spike timing in auditory cortex. *Nature* 426, 442–446.
- Wilent, W.B., and Contreras, D. (2005). Dynamics of excitation and inhibition underlying stimulus selectivity in rat somatosensory cortex. *Nat. Neurosci.* 8, 1364–1370.
- Willmore, B., and Tolhurst, D.J. (2001). Characterizing the sparseness of neural codes. *Network* 12, 255–270.
- Wilson, D.A., Kadohisa, M., and Fletcher, M.L. (2006). Cortical contributions to olfaction: plasticity and perception. *Semin. Cell Dev. Biol.* 17, 462–470.
- Zou, Z., Li, F., and Buck, L.B. (2005). Odor maps in the olfactory cortex. *Proc. Natl. Acad. Sci. USA* 102, 7724–7729.